NANO LETTERS

pubs.acs.org/NanoLett

Letter

Proximity Matters: Interfacial Solvation Dictates Solid Electrolyte Interphase Composition

Solomon T. Oyakhire, Sheng-Lun Liao, Sanzeeda Baig Shuchi, Mun Sek Kim, Sang Cheol Kim, Zhiao Yu, Rafael A. Vilá, Paul E. Rudnicki, Yi Cui,* and Stacey F. Bent*

Cite This: *Nano Lett.* 2023, 23, 7524–7531

Read Online

ACCESS | Metrics & More | Article Recommendations | Supporting Information

ABSTRACT: The composition of the solid electrolyte interphase (SEI) plays an important role in controlling Li–electrolyte reactions, but the underlying cause of SEI composition differences between electrolytes remains unclear. Many studies correlate SEI composition with the bulk solvation of Li ions in the electrolyte, but this correlation does not fully capture the interfacial phenomenon of SEI formation. Here, we provide a direct connection between SEI composition and Li-ion solvation by forming SEIs using polar substrates that modify interfacial solvation structures. We circumvent the deposition of Li metal by forming the SEI above Li^+/Li redox potential. Using theory, we show that an increase in the probability density of anions near a polar substrate increases anion incorporation within the SEI, providing a direct correlation between interfacial solvation and SEI composition. Finally, we use this concept to form stable anion-rich SEIs, resulting in high performance lithium metal batteries.

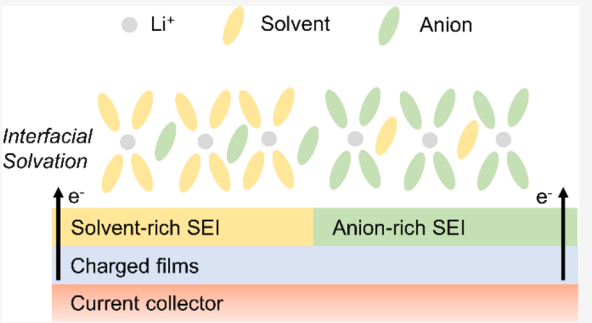

KEYWORDS: *solid electrolyte interphase formation, interfacial solvation, lithium metal batteries, atomic layer deposition, polar substrates*

Lithium metal batteries (LMBs) hold the potential to revolutionize energy storage owing to the high gravimetric capacity of Li (3860 mAh/g).[1] However, LMBs are often plagued with significant capacity losses due to the high reducing power of Li.[1] Practically, these capacity losses result partly from Li–electrolyte reactions which form an interfacial film known as the solid electrolyte interphase (SEI).[2] The extent of the Li–electrolyte reaction is usually related to the quality of the SEI formed from electrolyte decomposition at the Li–electrolyte interface. High quality SEIs lead to significant reductions in Li reactions and lower capacity loss. Thus, to quell Li–electrolyte reactions and reduce capacity loss in LMBs, electrolyte engineering has become a leading strategy for tuning SEI quality.[3−7]

In electrolyte engineering, the control of electrolyte solvation (the distribution of cations and anions in the presence of solvents) has emerged as an important tool for controlling the quality of SEIs.[3,4,6,8,9] Because the quality of an SEI is dependent on its properties, recent work has focused on modifying its chemistry and structure by changing the electrolyte solvation. The motivation for solvation modification is that certain Li salts decompose into species like LiF which are speculated to be beneficial for the passivation (a reduction in the extent of reaction) of Li metal.[5,10] Hence, to promote the passivation of Li metal, electrolyte engineering strategies have been targeted at promoting Li^+ solvation environments that are rich in the corresponding F-containing anions of Li salts. This solvation principle has resulted in numerous classes of promising electrolytes such as high concentration electrolytes in which Li^+–anion coordination is promoted by increasing salt concentration;[11] localized high concentration electrolytes in which Li^+–anion coordination is further promoted by the presence of a nonsolvating diluent;[12,13] and weakly solvating molecules which coordinate with Li^+ minimally, resulting in strong Li^+–anion coordination.[3,4] While the benefits of modifying Li^+ solvation have been demonstrated by significant improvements in LMB performance, the mechanistic pathway from electrolyte solvation to SEI formation remains unclear.

A key reason it is difficult to substantiate the connection between electrolyte solvation and the ensuing SEI composition is because solvation is measured in the bulk electrolyte rather than at the interface of Li where the SEI forms. Solvation studies are often performed using techniques like molecular dynamics (MD) simulations[3,4] and Raman spectroscopy.[14,15] These techniques are applied to bulk snapshots of LMB electrolytes, and the anion prevalence within Li^+ vicinity is

Received: May 31, 2023
Revised: August 1, 2023
Published: August 11, 2023

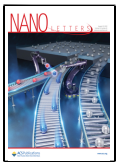

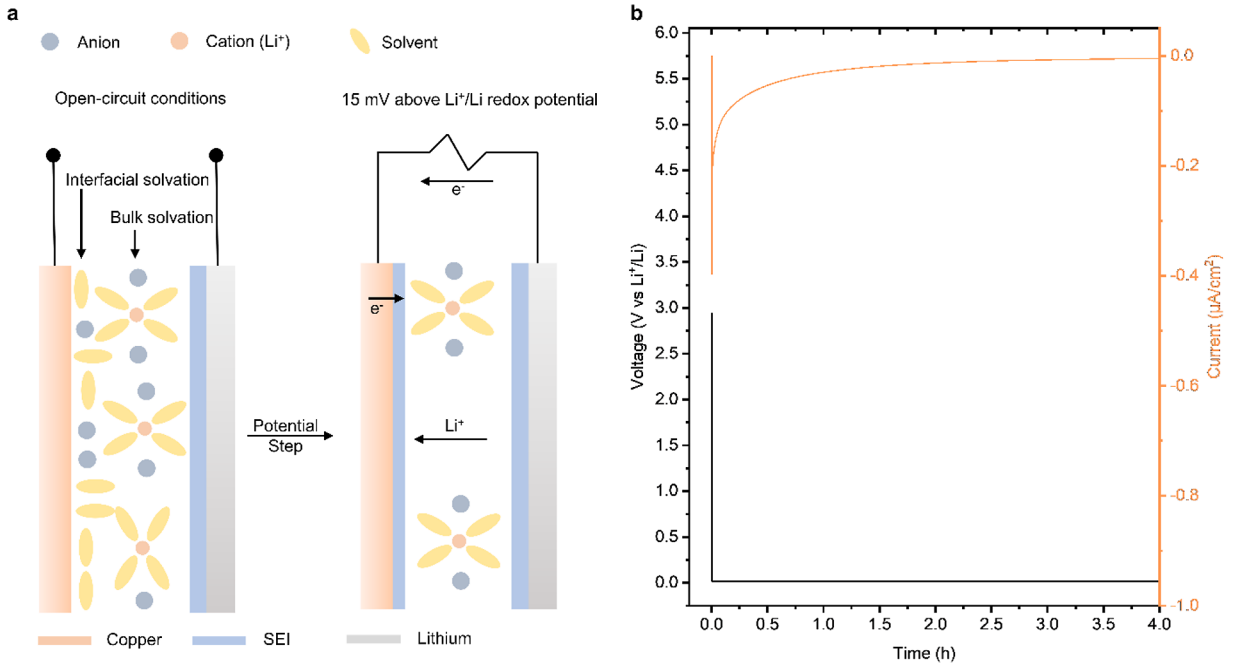

Figure 1. Conceptual framework for potential step experiments. (a) Schematic representation of the SEI formation experiment. (b) Depiction of typical voltage and current trends during the SEI formation experiment.

calculated based on the immediate coordination environment of Li^+. While bulk electrolyte measurements offer some understanding of SEI formation, they do not present a comprehensive mechanistic view as they overlook interfacial solvation at the Li−electrolyte interface, which is where the SEI is formed. Given that electrolyte solvation plays a vital role in the advancement of LMBs, it is crucial to elucidate the solvation−SEI pathway by using well-defined principles.

Our work clarifies the solvation−SEI dilemma by providing the first causal relationship between SEI composition and interfacial solvation in LMBs. By using stable substrates for SEI formation, we make a direct connection between solvation behavior near the electrolyte/substrate interface and the resulting SEI. We achieve a stable substrate by using Al_2O_3 films, which alter interfacial solvation by increasing the anion density near current collector substrates. The anion-rich solvation environment of Al_2O_3 influences electrolyte decomposition by promoting the formation of anion-rich SEIs. By pairing interfacial MD simulations with spectroscopy tools, we verify the existence of the SEI−solvation relationship. To demonstrate the generalizability of this relationship, we report similar SEI chemistry changes in three distinct classes of electrolytes. We show that interfacial solvation matters during SEI formation because the density of species near an electrode is positively correlated to their likelihood of becoming incorporated in the SEI. Finally, we demonstrate that the SEI formed prior to Li deposition impacts electrochemical performance after Li deposition, resulting in Coulombic efficiency (CE) improvements of up to 0.3% over a state-of-the-art electrolyte (99.4%). Our work clarifies the relationship between electrolyte solvation and SEI composition, resulting in a discovery that can be applied to the design of better LMBs.

To form the SEI, we apply a potential step from open-circuit conditions to 15 mV above the Li^+/Li redox potential in Li||Cu cells. The typical current response expected for this kind of potential step measurement is shown in Figure 1b, in which current increases immediately after the potential step, commensurate with formation of an SEI, and then it decreases gradually as the electrode surface becomes passivated (nonconductive to electron transport). By holding the potential at 15 mV vs Li^+/Li for 24 h, we prevent Li deposition while promoting the decomposition of solvents and anions in typical liquid electrolytes.[16] And, by operating close to the Li^+/Li redox potential, the electrons in Cu possess an electrochemical potential similar to those in deposited Li. The prevention of Li deposition and the preservation of electron energy make this platform suitable for understanding the kinetics of SEI formation atop Li. Figure 1a provides a conceptual illustration of the electrolyte species expected during the experiment, showing that the species likely adopt different configurations close to the surface of Cu compared with those in the bulk electrolyte. Moreover, another benefit of this SEI formation platform is that by modifying the surface of Cu, interfacial solvation of the electrolyte can be systematically changed. This benefit enables connections between interfacial solvation and SEI chemistry after potential step experiments.

To examine the effects of solvation on SEI formation, material selection for Cu modification is important. In this work, Al_2O_3 was selected as the interfacial film for two reasons: First, we previously demonstrated that it is electrochemically stable close to the Li^+/Li redox potential,[16] indicating that Al_2O_3 can serve as a stable electron transport mediator during SEI formation. Second, it is a polar film,[19] implying that it can promote preferential anion adsorption and alter interfacial solvation near the current collector interface. The thin films of Al_2O_3 were deposited onto Cu using atomic layer deposition (ALD) to ensure coating conformality atop Cu.

The electrochemical stability of the Al_2O_3 films is substantiated by using linear sweep voltammetry (LSV) and X-ray photoelectron spectroscopy (XPS) experiments. Both the LSV and XPS experiments were performed with a widely used electrolyte consisting of 1 M lithium hexafluorophosphate ($LiPF_6$) in a 1:1 volume ratio of ethylene carbonate (EC) and diethyl carbonate (DEC) (denoted as LP40 hereafter). First,

https://doi.org/10.1021/acs.nanolett.3c02037
Nano Lett. 2023, 23, 7524−7531

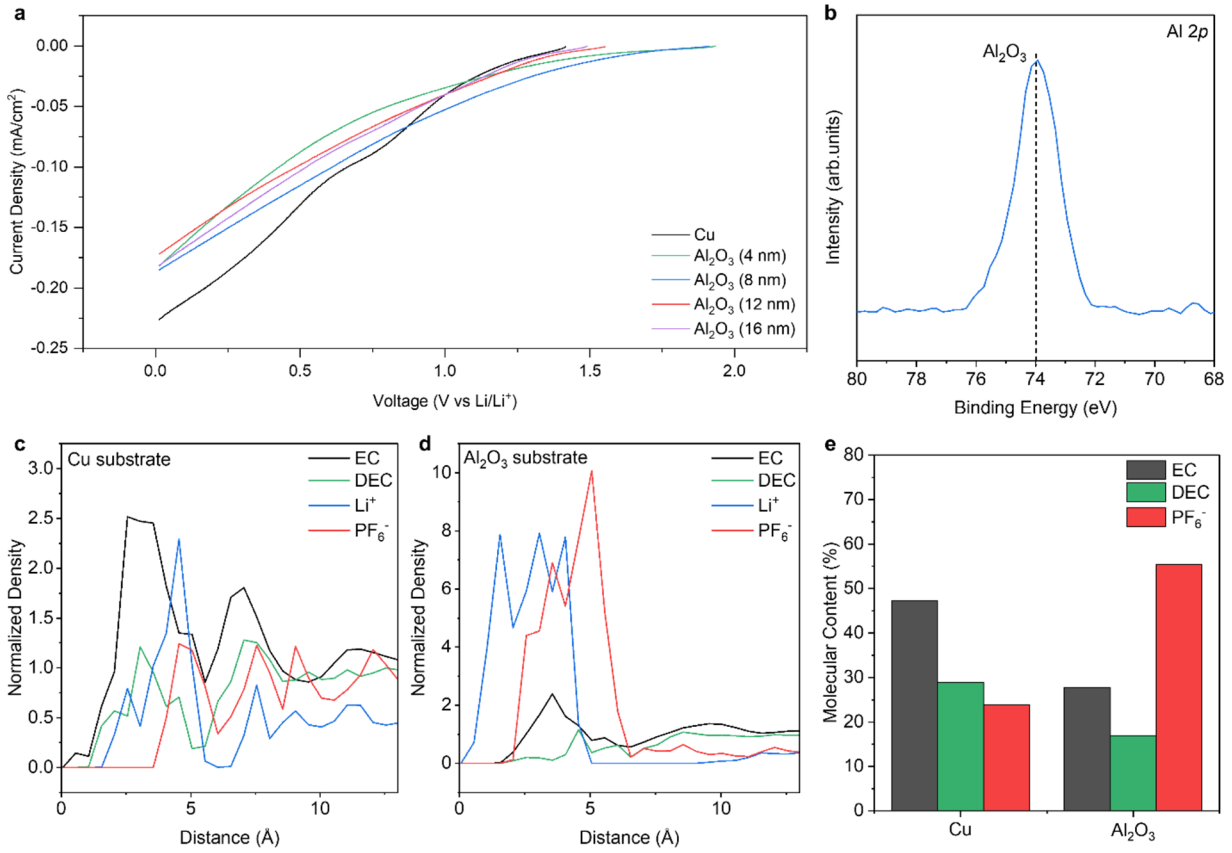

Figure 2. Electrochemical stability and solvation properties of Cu and Al_2O_3 substrates. (a) Measured current density as a function of voltage during potential sweeps at 5 mV/s in LP40 from OCV to 15 mV vs Li^+/Li for Cu and Al_2O_3 substrates. (b) XPS high-resolution spectrum of Al_2O_3, collected after a 24 h hold in LP40 at 15 mV vs Li^+/Li. (c, d) Normalized probability density of electrolyte species within the vicinity of the Cu and Al_2O_3 substrates, respectively, determined by MD simulations. (e) Molecular content of species near both substrates calculated based on probability densities in panels c and d.

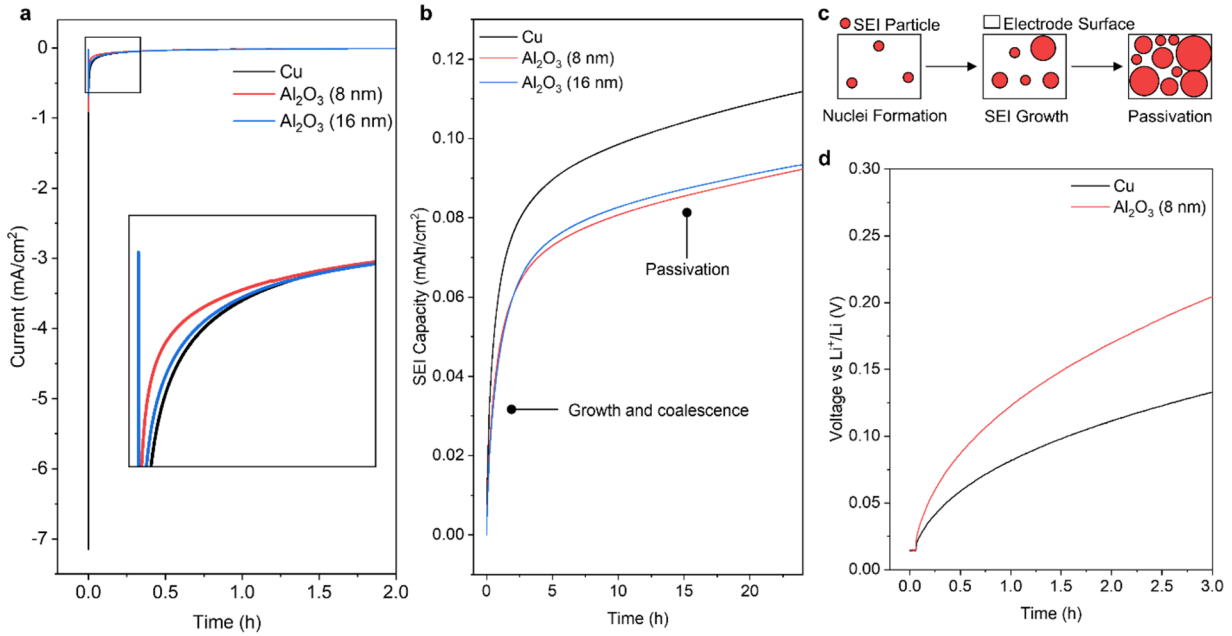

Figure 3. SEI formation mechanism atop substrates. (a) Current−time trends for SEI formation in LP40 on Cu and Al_2O_3 substrates. The inset shows current−time trends for all substrates within a short time scale. (b) SEI capacity as a function of time for Cu and Al_2O_3 substrates, obtained by integrating current over time for data displayed in panel a. (c) Illustration of SEI particle formation and growth mechanism on both Cu and Al_2O_3 substrates. (d) Voltage relaxation tests showing substrate voltage vs Li^+/Li as a function of relaxation time after 24 h of SEI formation in LP40 on different substrates.

https://doi.org/10.1021/acs.nanolett.3c02037
Nano Lett. 2023, 23, 7524−7531

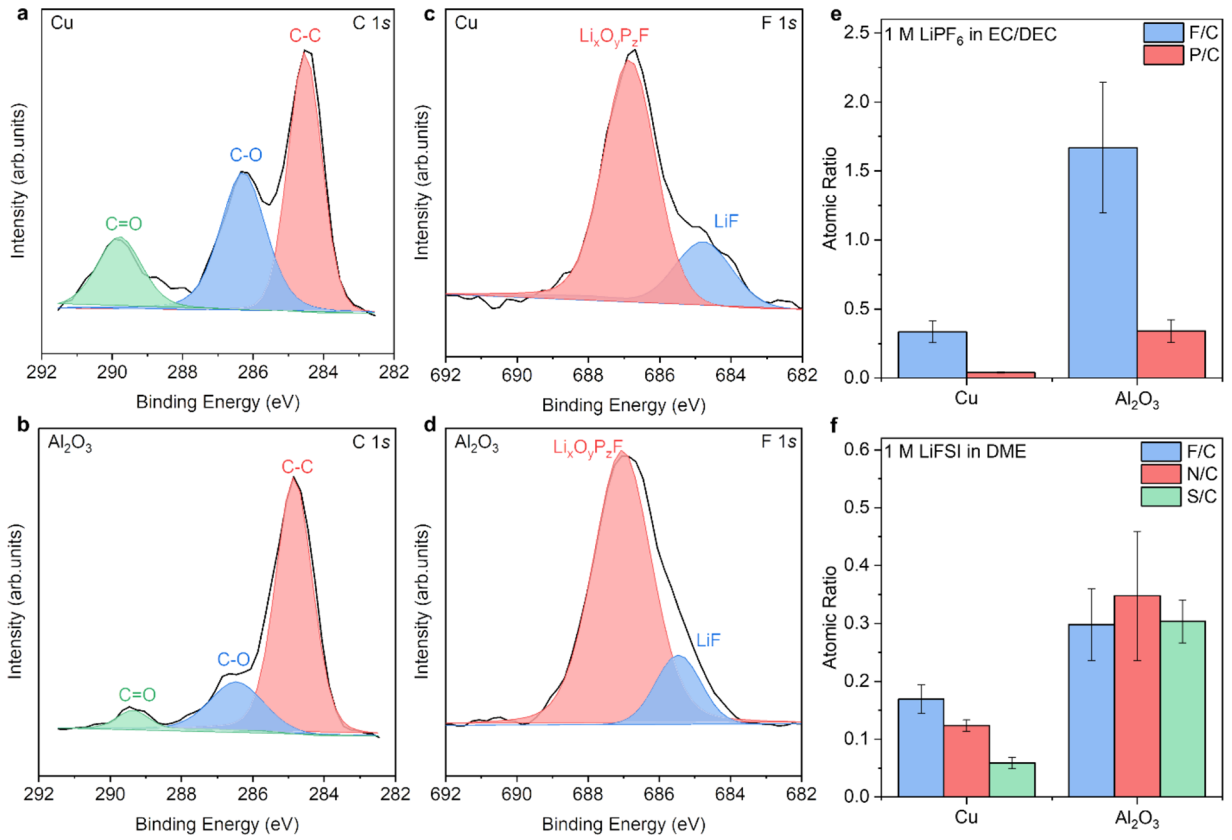

Figure 4. SEI chemistry and speciation in different electrolytes. (a, b) High-resolution C 1s XPS peaks of SEIs formed in LP40 on Cu and Al_2O_3 substrates, respectively. (c, d) High-resolution F 1s XPS peaks of SEIs formed in LP40 on Cu and Al_2O_3 substrates, respectively. (e, f) Atomic ratio of SEIs formed on Cu and Al_2O_3 substrates in LP40 and 1 M LiFSI/DME electrolytes, respectively.

by scanning at 5 mV/s from open-circuit voltage (OCV) to 15 mV vs Li^+/Li, we do not observe reduction peaks that are different from those of Cu for four film thicknesses of Al_2O_3 (4, 8, 12, and 16 nm), indicating that the films remain stable during the potential sweep (Figure 2a). In addition, no increase in current is observed with an increase in Al_2O_3 film thickness, as would be expected if the films were undergoing electrochemical conversion, suggesting that the films remain stable (Figure 2a). To confirm that the Al_2O_3 film stability is maintained over the typical duration of our SEI formation experiments, we perform XPS after SEI formation on Al_2O_3 at 15 mV vs Li^+/Li for 24 h. At the end of the 24 h hold, the Al 2p XPS peak in the Al_2O_3 film is detected at 74 eV, consistent with the binding energy of Al in Al_2O_3 (Figure 2b and Figure S1). If Al_2O_3 is reduced, its Al 2p binding energy would be less than 74 eV.

We investigate the effects of the Al_2O_3 polarity on electrolyte solvation by using MD simulations to quantify the interfacial distribution of electrolyte species on Cu and Al_2O_3 substrates. MD simulations were performed in a box filled with LP40 electrolyte situated atop Cu and Al_2O_3 substrates. Figures 2c and 2d show the normalized probability density of the electrolyte species as a function of distance away from both Cu and Al_2O_3 substrates. We normalized the probability densities of species near the substrates with respect to bulk electrolyte densities (defined as species located >13 Å away from each substrate) to provide a tractable basis for comparing interfacial densities between both substrates. Consequently, the solvation data captured within the first 13 Å of each substrate, shown in Figures 2c and 2d, reflect the effects of substrate surface charge on interfacial solvation. From the results, we observe that cations and anions (Li^+ and PF_6^-) are enriched within the vicinity of the Al_2O_3 substrate in comparison to the Cu substrate. This effect may be attributed to the Lewis acidic Al^{3+} sites of Al_2O_3[17] which attract electron dense PF_6^- species to the surface of Al_2O_3 and the Lewis basic sites of O^{2-} which attract electron-deficient Li^+ species. By quantifying the electrolyte species within 13 Å of each substrate (Figure 2e), we observe that solvents dominate the interfacial solvation of Cu with EC constituting 48% of molecular content, while the PF_6^- anion dominates the interfacial solvation of Al_2O_3, constituting 57% of molecular content.

To investigate if the changes in interfacial solvation identified in Figures 2c–e impact SEI formation, we study the electrochemical mechanism of SEI formation on both Cu and Al_2O_3-modified Cu. We apply a potential step from open circuit conditions to 15 mV vs Li^+/Li using Li|Cu cells with 30 μL of the LP40 electrolyte. The cells are subsequently fixed at 15 mV for 24 h to ensure complete passivation of the Cu surface. Representative current response profiles are shown in Figure 3a for Cu and Cu modified with 8 nm and 16 nm of Al_2O_3. Here, the magnitude of the instantaneous increase in current density differs because it is related to the electrical conductivity of the substrates, with the Cu, 8 nm Al_2O_3, and 16 nm Al_2O_3 substrates showing peak currents of −7, −0.9, and −0.7 mA/cm^2, respectively (Figure 3a). However, the current decay trend is similar across substrates, indicating that they form SEIs through similar mechanisms (inset to Figure 3a). By fitting the current decay curves in Figure 3a to nucleation and

https://doi.org/10.1021/acs.nanolett.3c02037
Nano Lett. 2023, 23, 7524−7531

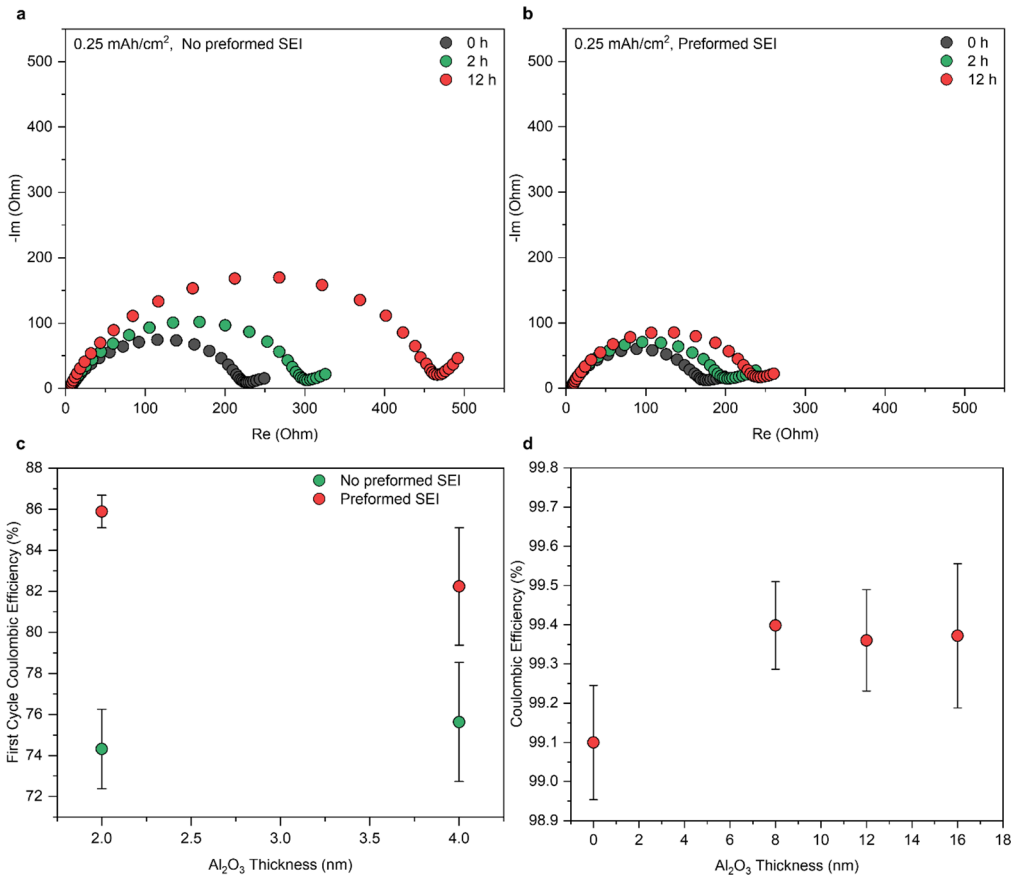

Figure 5. Electrochemical implications of anion-rich SEI. (a, b) Nyquist plot of impedance growth after 0.25 mAh/cm^2 of Li is deposited at 0.5 mA/cm^2 on Al_2O_3 substrates without and with preformed SEIs in LP40, respectively. The markers represent aging times of 0 h, 2 h, and 12 h. (c) First cycle CE after Li deposition and stripping on 2−4 nm thick Al_2O_3 substrates with and without preformed SEIs tested in LP40 at 0.5 mA/cm^2 and 0.5 mAh/cm^2. (d) Aurbach CE measurements for Cu and Al_2O_3 substrates with preformed SEIs tested in 1.2 M LiFSI F5DEE at 0.5 mA/cm^2. In (d), the Al_2O_3 film thickness is 8−16 nm.

growth models,[18,19] we find that the SEI formation mechanism for both substrates appears to follow 3D nucleation and growth (Figure S2 and Note 1 of the Supporting Information).

As further verification for the SEI formation mechanism, we integrate current over time during the potential hold to obtain the SEI capacity as a function of time (Figure 3b). Figure 3b shows that the SEI formation pathways for all substrates are similar, with an initial steep increase in the capacity followed by a slower increase in capacity. The formation mechanism suggested by the curves in Figure 3b is illustrated in Figure 3c. After the initial potential step, SEI particles nucleate on the substrate surface, leaving some parts of the substrate exposed (Figure 3c). As the potential hold continues, SEI particles coalesce, allowing electrolyte species to access the electrode surface for growth of existing SEI particles as well as formation of new SEI particles (Figure 3c). This SEI formation process continues until most of the Cu surface is covered (and hence passivated) (Figure 3c). The illustration of SEI formation shown in Figure 3c is consistent with those reported in other SEI formation studies.[20,21]

Even though the SEI formation pathways appear to be mechanistically similar across substrates, the elbow of the SEI capacity curve differs between them (Figure 3b). We hypothesize that the elbow serves as a proxy for Cu passivation. It is evident that the elbow occurs at a lower capacity (~0.07 mAh/cm^2) in the Al_2O_3-modified Cu than on bare Cu, in which it presents at ~0.09 mAh/cm^2 (Figure 3b). This elbow difference may be indicative of the high electrical resistance of Al_2O_3 which reduces the SEI thickness required to suppress electron transport. On the other hand, it may also be indicative of different SEI species formed atop both substrates because some SEI species are more electrically insulating than others.[2] While the electrical properties of Al_2O_3 are known and well-studied, the possible differences in SEI species formed atop Cu and Al_2O_3 substrates are unknown. To explore the possible differences in species, we perform a voltage relaxation test after 24 h of SEI formation atop Cu and 8 nm Al_2O_3 (Figure 3d). During the relaxation test, the measured potential versus Li^+/Li varies between substrates, with the Al_2O_3 substrate displaying a higher potential than the Cu substrate (Figure 3d). Similar differences in relaxation potential are observed between both substrates even after 1 h of SEI formation (Figure S3). These differences in relaxation potential could arise from differences in composition of SEIs formed on both substrates.

We carry out XPS on the substrates after 24 h of SEI formation to examine the chemical composition of SEIs formed atop them. As shown in Figures 4a and 4b, characteristic C−C, C−O, and C═O species are formed on both substrates, indicating decomposition of solvent species in the LP40 electrolyte. Similarly, the F 1s species (LiF and $Li_xO_yP_zF$) formed on both substrates are the same (Figures 4c,d). The identification of similar species within the SEIs is not unexpected because the SEI was formed at the same

https://doi.org/10.1021/acs.nanolett.3c02037
Nano Lett. 2023, 23, 7524−7531

potential on both substrates using the same electrolyte. To probe the SEI chemistry further, we performed detailed elemental analysis of the ratios of species present in the SEI. The elemental composition of the SEI could indicate the contribution of anions and solvents to SEI formation. For instance, the LP40 electrolyte contains F, O, C, and P, with P and F being unique elements of the PF_6 anion and C and O being unique elements of the EC and DEC solvents. Hence, by calculating the ratio of P/C and F/C, the relative contribution of anions to solvents during SEI formation can be inferred.[22,23] In Figure 4e, we present the F/C and P/C ratios in SEIs formed on top of Cu and Al_2O_3 substrates. When compared to the Cu substrate, the SEI formed on Al_2O_3 possesses higher quantities of anion-derived SEI species, with F/C and P/C ratios of 1.6 and 0.3, respectively, in comparison to 0.35 and 0.05 on Cu. Because the electrolyte used on both substrates is the same, this difference in SEI speciation suggests that the interfacial environment near the Al_2O_3 substrate increases the rate of anion decomposition. This finding is important for SEI design because it provides concrete chemical evidence that interfacial solvation changes directly translate into SEI differences. The importance of interfacial solvation in SEI formation was recently demonstrated in a computational study as well.[24]

We demonstrate that this increase in anion-derived ratios generalizes to other electrolytes such as 1 M lithium bisfluorosulfonyl imide (LiFSI) in dimethoxyethane (DME) and 1 M LiFSI in fluorinated 1,4-dimethoxylbutane (FDMB) electrolytes (Figure 4f and Figure S4). As additional evidence for generalizability, we show that the SEI chemistry differences between Cu and Al_2O_3 exist even after 1 h of SEI formation, and when the thickness of Al_2O_3 is increased from 8 to 16 nm (Figure S5).

To examine the electrochemical implications of the SEI preformed on Al_2O_3, we perform 12 h aging experiments on Li deposited atop 8 nm Al_2O_3 substrates of two types—those with preformed SEIs and those without preformed SEIs. We do not examine the electrochemical implications of the SEI formed on Cu here because our previous work examined that in detail.[23] By using electrochemical impedance spectroscopy (EIS) to measure the impedance of the Li deposits within the first 12 h of aging, we observe that the Al_2O_3 substrates without preformed SEIs display 100% increase in impedance while the substrates with preformed SEIs display 33% increase in impedance (Figures 5a,b). This finding shows that the corrosion of deposited Li is significantly reduced when Li is deposited on the substrate with an anion-rich preformed SEI. SEM images indicate that the Li morphologies formed on Al_2O_3 in the presence and absence of SEI preformation are similar (Figure S6), suggesting that the reduced Li−electrolyte reactions are not due to differences in Li contact area but rather the anion-rich nature of the preformed SEI.

The benefits of this anion-rich interphase are reflected in first cycle CE experiments in which SEI preformation improves CE by as much as 12% (Figure 5c). For these first cycle CE tests, thin films of Al_2O_3 (2 and 4 nm) were used to reduce morphology and performance improvements that are associated with thicker Al_2O_3 films (>8 nm).[25] Next, using 1.2 M LiFSI in 2-(2-(2,2-difluoroethoxy)ethoxy)-1,1,1-trifluoroethane (F5DEE), we combine SEI preformation benefits with improved morphologies in the thicker films (8−16 nm Al_2O_3) and compare the resulting CEs with that from a Cu substrate without Al_2O_3 (thickness = 0 nm data point). This test is intended to further demonstrate the benefits of the preformed SEI in a state-of-the-art cell that contains the F5DEE electrolyte and >8 nm thick Al_2O_3 films. The data reveal an average improvement of ∼0.3% in CE measured using the Aurbach method[26] performed at 0.5 mA/cm^2 (Figure 5d). The 8−16 nm Al_2O_3 films show similar CE, likely because they form similar SEIs and lithium morphologies. A lower CE is obtained when the 8 nm Al_2O_3 film is cycled without preformation in the F5DEE electrolyte (Figure S7), showing that preformation is beneficial. The findings in Figures 5c,d are supported by the voltage profiles presented in Figure S8.

In summary, we have shown that proximity matters during SEI formation because electrolyte species that are close to a reducing electrode are likely to become incorporated in the SEI during electrolyte decomposition. By using Cu and Cu modified with Al_2O_3, we show that the interfacial solvation of electrolyte species varies with the substrate chemistry and polarity. Specifically, an increased anion density near the Al_2O_3-modified substrate surface correlates with an increase in the incorporation of anions into the SEI during electrolyte decomposition. We also reveal similar SEI formation mechanisms between Cu and Al_2O_3-modified Cu. This suggests that the observed variations in SEI chemistry could be attributed to changes in interfacial solvation rather than differences in the SEI formation mechanism. The combined insights from the SEI formation mechanism, anion density within the vicinity of substrates, and SEI chemistry differences between substrates provide the first direct correlation between interfacial solvation and SEI speciation. We extend the correlation to three distinct electrolytes and show consistently that the Al_2O_3-modified substrate increases anion incorporation in the SEI. Finally, we demonstrate that the anion-rich SEI formed atop Al_2O_3 provides electrochemical benefits even after Li deposition, as evidenced by reduced Li corrosion and improved battery efficiency. This work provides an important relationship between electrolyte solvation and SEI formation that is relevant for improving the performance of LMBs.

■ ASSOCIATED CONTENT

Supporting Information

The Supporting Information is available free of charge at https://pubs.acs.org/doi/10.1021/acs.nanolett.3c02037.

Description of all methods used in the paper, additional details on models for SEI growth, XPS spectra and atomic ratios for Al_2O_3 substrates and SEIs, additional voltage profiles, SEM images of lithium deposits (PDF)

■ AUTHOR INFORMATION

Corresponding Authors

Yi Cui − *Department of Materials Science and Engineering and Department of Energy Science and Engineering, Stanford University, Stanford, California 94305, United States; Stanford Institute for Materials and Energy Sciences, SLAC National Accelerator Laboratory, Menlo Park, California 94025, United States;* orcid.org/0000-0002-6103-6352; Email: yicui@stanford.edu

Stacey F. Bent − *Department of Chemical Engineering, Stanford University, Stanford, California 94305, United States; Department of Energy Science and Engineering, Stanford University, Stanford, California 94305, United States;* orcid.org/0000-0002-1084-5336; Email: sbent@stanford.edu

https://doi.org/10.1021/acs.nanolett.3c02037
Nano Lett. 2023, 23, 7524−7531

Authors

Solomon T. Oyakhire − *Department of Chemical Engineering, Stanford University, Stanford, California 94305, United States;* orcid.org/0000-0002-3189-5949

Sheng-Lun Liao − *Department of Chemical Engineering, Stanford University, Stanford, California 94305, United States*

Sanzeeda Baig Shuchi − *Department of Chemical Engineering, Stanford University, Stanford, California 94305, United States*

Mun Sek Kim − *Department of Chemical Engineering, Stanford University, Stanford, California 94305, United States; Department of Materials Science and Engineering, Stanford University, Stanford, California 94305, United States*

Sang Cheol Kim − *Department of Materials Science and Engineering, Stanford University, Stanford, California 94305, United States;* orcid.org/0000-0002-1749-8277

Zhiao Yu − *Department of Chemistry, Stanford University, Stanford, California 94305, United States;* orcid.org/0000-0001-8746-1640

Rafael A. Vilá − *Department of Materials Science and Engineering, Stanford University, Stanford, California 94305, United States*

Paul E. Rudnicki − *Department of Chemical Engineering, Stanford University, Stanford, California 94305, United States;* orcid.org/0000-0003-3518-1721

Complete contact information is available at: https://pubs.acs.org/10.1021/acs.nanolett.3c02037

Author Contributions

S.T.O. conceived the idea and designed the experiments. S.T.O. performed the experiments under the guidance of Y.C. and S.F.B. S.T.O. performed electrochemistry experiments, ALD, and XPS. S.T.O. analyzed and interpreted all results. S-L.L. performed MD simulations. S.B.S. assisted with all experiments. M.S.K., S.C.K., and R.A.V. contributed to key discussions. Z.Y. synthesized and provided the F5DEE electrolyte. P.E.R. assisted with setting up the MD simulations. Y.C. and S.F.B. supervised the project. S.T.O. wrote the manuscript and revised it based on input from Y.C. and S.F.B. All authors read and discussed the manuscript.

Notes

The authors declare no competing financial interest.

■ ACKNOWLEDGMENTS

S.T.O. acknowledges support from the Knight-Hennessy scholarship for graduate studies at Stanford University and the TomKat Center Fellowship for Translational Research at Stanford University. S.B.S. acknowledges support from the Stanford University StorageX seed grant award. R.A.V. acknowledges support from the National Academy of Sciences Ford Foundation Fellowship, the National Science Foundation Graduate Research Fellowship Program (NSF GRFP, Grant DGE-1656518), and the Enhancing Diversity in Graduate Education (EDGE) Doctoral Fellowship Program at Stanford University. Y.C. acknowledges support from the Assistant Secretary for Energy Efficiency and Renewable Energy, Office of Vehicle Technologies, of the U.S. Department of Energy under the Battery Materials Research (BMR) Program and the Battery500 Consortium program. Part of this work was performed at the Stanford Nano Shared Facilities (SNSF), supported by the National Science Foundation under Award ECCS-2026822.

■ REFERENCES

(1) Lin, D.; Liu, Y.; Cui, Y. Reviving the Lithium Metal Anode for High-Energy Batteries. *Nat. Nanotechnol.* **2017**, *12* (3), 194−206.

(2) Peled, E.; Menkin, S. Review—SEI: Past, Present and Future. *J. Electrochem. Soc.* **2017**, *164* (7), A1703−A1719.

(3) Yu, Z.; Wang, H.; Kong, X.; Huang, W. W.; Tsao, Y.; Mackanic, D. G.; Wang, K.; Wang, X.; Huang, W. W.; Choudhury, S.; Zheng, Y.; Amanchukwu, C. V.; Hung, S. T.; Ma, Y.; Lomeli, E. G.; Qin, J.; Cui, Y.; Bao, Z. Molecular Design for Electrolyte Solvents Enabling Energy-Dense and Long-Cycling Lithium Metal Batteries. *Nat. Energy* **2020**, *5* (7), 526−533.

(4) Yu, Z.; Rudnicki, P. E.; Zhang, Z.; Huang, Z.; Celik, H.; Oyakhire, S. T.; Chen, Y.; Kong, X.; Kim, S. C.; Xiao, X.; Wang, H.; Zheng, Y.; Kamat, G. A.; Kim, M. S.; Bent, S. F.; Qin, J.; Cui, Y.; Bao, Z. Rational Solvent Molecule Tuning for High-Performance Lithium Metal Battery Electrolytes. *Nat. Energy* **2022**, *7* (1), 94−106.

(5) Zhang, X.-Q.; Cheng, X.-B.; Chen, X.; Yan, C.; Zhang, Q. Fluoroethylene Carbonate Additives to Render Uniform Li Deposits in Lithium Metal Batteries. *Adv. Funct. Mater.* **2017**, *27* (10), 1605989.

(6) Kim, M. S.; Zhang, Z.; Rudnicki, P. E.; Yu, Z.; Wang, J.; Wang, H.; Oyakhire, S. T.; Chen, Y.; Kim, S. C.; Zhang, W.; Boyle, D. T.; Kong, X.; Xu, R.; Huang, Z.; Huang, W.; Bent, S. F.; Wang, L.-W.; Qin, J.; Bao, Z.; Cui, Y. Suspension Electrolyte with Modified Li+ Solvation Environment for Lithium Metal Batteries. *Nat. Mater.* **2022**, *21* (4), 445−454.

(7) Cao, X.; Ren, X.; Zou, L.; Engelhard, M. H.; Huang, W.; Wang, H.; Matthews, B. E.; Lee, H.; Niu, C.; Arey, B. W.; Cui, Y.; Wang, C.; Xiao, J.; Liu, J.; Xu, W.; Zhang, J.-G. G. Monolithic Solid-Electrolyte Interphases Formed in Fluorinated Orthoformate-Based Electrolytes Minimize Li Depletion and Pulverization. *Nat. Energy* **2019**, *4* (9), 796−805.

(8) Zhang, X. Q.; Chen, X.; Hou, L. P.; Li, B. Q.; Cheng, X. B.; Huang, J. Q.; Zhang, Q. Regulating Anions in the Solvation Sheath of Lithium Ions for Stable Lithium Metal Batteries. *ACS Energy Lett.* **2019**, *4* (2), 411−416.

(9) Kim, S. C.; Kong, X.; Vilá, R. A.; Huang, W.; Chen, Y.; Boyle, D. T.; Yu, Z.; Wang, H.; Bao, Z.; Qin, J.; Cui, Y. Potentiometric Measurement to Probe Solvation Energy and Its Correlation to Lithium Battery Cyclability. *J. Am. Chem. Soc.* **2021**, *143* (27), 10301−10308.

(10) Huang, W.; Wang, H.; Boyle, D. T.; Li, Y.; Cui, Y. Resolving Nanoscopic and Mesoscopic Heterogeneity of Fluorinated Species in Battery Solid-Electrolyte Interphases by Cryogenic Electron Microscopy. *ACS Energy Lett.* **2020**, *5* (4), 1128−1135.

(11) Qian, J.; Henderson, W. A.; Xu, W.; Bhattacharya, P.; Engelhard, M.; Borodin, O.; Zhang, J. G. High Rate and Stable Cycling of Lithium Metal Anode. *Nat. Commun.* **2015**, *6* (1), 1−9.

(12) Ren, X.; Chen, S.; Lee, H.; Mei, D.; Engelhard, M. H.; Burton, S. D.; Zhao, W.; Zheng, J.; Li, Q.; Ding, M. S.; Schroeder, M.; Alvarado, J.; Xu, K.; Meng, Y. S.; Liu, J.; Zhang, J. G.; Xu, W. Localized High-Concentration Sulfone Electrolytes for High-Efficiency Lithium-Metal Batteries. *Chem.* **2018**, *4* (8), 1877−1892.

(13) Chen, S.; Zheng, J.; Mei, D.; Han, K. S.; Engelhard, M. H.; Zhao, W.; Xu, W.; Liu, J.; Zhang, J.-G. High-Voltage Lithium-Metal Batteries Enabled by Localized High-Concentration Electrolytes. *Adv. Mater.* **2018**, *30* (21), 1706102.

(14) Lee, S. H.; Hwang, J. Y.; Ming, J.; Cao, Z.; Nguyen, H. A.; Jung, H. G.; Kim, J.; Sun, Y. K. Toward the Sustainable Lithium Metal Batteries with a New Electrolyte Solvation Chemistry. *Adv. Energy Mater.* **2020**, *10* (20), 2000567.

(15) Chang, Z.; Qiao, Y.; Deng, H.; Yang, H.; He, P.; Zhou, H. A Liquid Electrolyte with De-Solvated Lithium Ions for Lithium-Metal Battery. *Joule* **2020**, *4* (8), 1776−1789.

(16) Huang, W.; Boyle, D. T.; Li, Y. Y.; Li, Y. Y.; Pei, A.; Chen, H.; Cui, Y. Nanostructural and Electrochemical Evolution of the Solid-

Electrolyte Interphase on CuO Nanowires Revealed by Cryogenic-Electron Microscopy and Impedance Spectroscopy. *ACS Nano* **2019**, *13* (1), 737−744.
(17) Sohlberg, K.; Pantelides, S. T.; Pennycook, S. J. Surface Reconstruction and the Difference in Surface Acidity between γ- and η-Alumina. *J. Am. Chem. Soc.* **2001**, *123* (1), 26−29.
(18) Scharifker, B.; Hills, G. Theoretical and Experimental Studies of Multiple Nucleation. *Electrochim. Acta* **1983**, *28* (7), 879−889.
(19) Bewick, A.; Fleischmann, M.; Thirsk, H. R. Kinetics of the Electrocrystallization of Thin Films of Calomel. *Trans. Faraday Soc.* **1962**, *58* (0), 2200−2216.
(20) Yao, Y. X.; Wan, J.; Liang, N. Y.; Yan, C.; Wen, R.; Zhang, Q. Nucleation and Growth Mode of Solid Electrolyte Interphase in Li-Ion Batteries. *J. Am. Chem. Soc.* **2023**, *145* (14), 8001−8006.
(21) Yan, C.; Jiang, L.-L. L.; Yao, Y.-X. X.; Lu, Y.; Huang, J.-Q. Q.; Zhang, Q. Nucleation and Growth Mechanism of Anion-Derived Solid Electrolyte Interphase in Rechargeable Batteries. *Angew. Chemie - Int. Ed.* **2021**, *60* (15), 8521−8525.
(22) Oyakhire, S. T.; Gong, H.; Cui, Y.; Bao, Z.; Bent, S. F. An X-Ray Photoelectron Spectroscopy Primer for Solid Electrolyte Interphase Characterization in Lithium Metal Anodes. *ACS Energy Lett.* **2022**, *7* (8), 2540−2546.
(23) Oyakhire, S. T.; Zhang, W.; Yu, Z.; Holmes, S. E.; Sayavong, P.; Kim, S. C.; Boyle, D. T.; Kim, M. S.; Zhang, Z.; Cui, Y.; Bent, S. F. Correlating the Formation Protocols of Solid Electrolyte Interphases with Practical Performance Metrics in Lithium Metal Batteries. *ACS Energy Lett.* **2023**, *8* (1), 869−877.
(24) Wu, Q.; McDowell, M. T.; Qi, Y. Effect of the Electric Double Layer (EDL) in Multicomponent Electrolyte Reduction and Solid Electrolyte Interphase (SEI) Formation in Lithium Batteries. *J. Am. Chem. Soc.* **2023**, *145* (4), 2473−2484.
(25) Oyakhire, S. T.; Zhang, W.; Shin, A.; Xu, R.; Boyle, D. T.; Yu, Z.; Ye, Y.; Yang, Y.; Raiford, J. A.; Huang, W.; Schneider, J. R.; Cui, Y.; Bent, S. F. Electrical Resistance of the Current Collector Controls Lithium Morphology. *Nat. Commun.* **2022**, *13* (1), 1−12.
(26) Adams, B. D.; Zheng, J.; Ren, X.; Xu, W.; Zhang, J.-G. G. Accurate Determination of Coulombic Efficiency for Lithium Metal Anodes and Lithium Metal Batteries. *Adv. Energy Mater.* **2018**, *8* (7), 1702097.

https://doi.org/10.1021/acs.nanolett.3c02037
Nano Lett. 2023, 23, 7524−7531